PHYSICS

Dalton's and Amagat's laws fail in gas mixtures with shock propagation

P. Wayne[1]*, S. Cooper[2], D. Simons[3], I. Trueba-Monje[4], D. Freelong[1], G. Vigil[1], P. Vorobieff[1], C. R. Truman[1], V. Vorob'ev[5], T. Clark[1]

A shock propagating through a gas mixture leads to pressure, temperature, and density increases across the shock front. Rankine-Hugoniot relations correlating pre- and post-shock quantities describe a calorically perfect gas but deliver a good approximation for real gases, provided the pre-shock conditions are well characterized with a thermodynamic mixing model. Two classic thermodynamic models of gas mixtures are Dalton's law of partial pressures and Amagat's law of partial volumes. We measure post-shock temperature and pressure in experiments with nonreacting binary mixtures of sulfur hexafluoride and helium (two dramatically disparate gases) and show that neither model can accurately predict the observed values, on time scales much longer than that of the shock front passage, due to the models' implicit assumptions about mixture behavior on the molecular level. However, kinetic molecular theory can help account for the discrepancy. Our results provide starting points for future theoretical work, experiments, and code validation.

INTRODUCTION

In 1802, John Dalton's publication in *Memoirs of the Literary and Philosophical Society of Manchester* formulated the law of additive (or partial) pressures (*1*), stating that the total pressure in a nonreactive gas mixture—at constant temperature and volume—is equal to the sum of the partial pressures of the component gases.

In 1880, French physicist Émile Hilaire Amagat published his findings while researching the compressibility of different gases (*2*). Amagat's law of partial volumes states that the total volume of a gas mixture is equal to the sum of the partial volumes each gas would occupy if it existed alone at the temperature and pressure of the mixture (*3*). While some advancements have been made in experiments of shock interaction with a single-component gas (*4*, *5*), much less is known about multicomponent gas mixtures.

Shock interactions with gas mixtures are relevant to many engineering problems, including gas-cooled reactor power plants (*6*, *7*), mixing processes in supersonic and hypersonic combustion (*8*–*11*), and astrophysical phenomena (*12*, *13*). Our experiment was originally designed to determine which thermodynamic law (Dalton or Amagat) is more suitable for predicting properties of gas mixtures interacting with a planar shock wave. Post-shock properties are obtained using the Rankine-Hugoniot equations (*14*–*18*), which calculate post-shock values, such as pressure, temperature, and density, based on incident shock Mach number and upstream (preshock) conditions.

For a proper comparison of theoretical and experimental values of post-shock properties, pressure and temperature must be measured immediately before (downstream of) and immediately after (upstream of) the shock front. Pressure measurements are not difficult: High-frequency response pressure transducers (PTs) are readily available. Temperature measurements are more challenging. Thermocouples are intrusive and lack the necessary response time [$\mathcal{O}(10^{-6}$ s)]. Infrared (IR) detectors, on the other hand, have ultrafast response times [$\mathcal{O}(10^{-8}$ s)] and are inherently nonintrusive. Here, we present temperature measurements using an InfraRed Associates mercury-cadmium-telluride (MCT), liquid nitrogen–cooled IR detector operating at 77 K, with a response time of 60 ns (6×10^{-8} s). Coupled with a Thorlabs stabilized broadband IR light source, with a color temperature of 1500 K, the MCT detector provides line-of-sight bulk temperature measurements both before and after the shock.

For our experiment, we selected two highly disparate gases forming a binary gas mixture: sulfur hexafluoride (SF_6) and helium (He). SF_6 and He are relatively inexpensive and nontoxic and have highly contrasting properties (molecular weight, viscosity, and specific heat), presenting an extreme (and hopefully easy to interpret) case of a mixture with easily distinguishable components. Two molar concentrations of each gas were chosen: 50%/50% (50/50) and 25%/75% (25/75) SF_6 to He, respectively.

The shock tube consists of two sections: driver and driven. The driver section is pressurized (with nitrogen) to a value depending on the desired strength of the shock wave. The driven section is pressurized with the test gas mixture, up to one of three different initial pressures: 39.3, 78.6, or 118 kPa (the average local atmospheric pressure in the laboratory is approximately 78.6 kPa). A thin-film polyester diaphragm separates the two sections. Once both sections have been evacuated using a vacuum pump, the driver is then filled with the driver gas, and the driven section is filled with our test gas mixture. When the driver and driven sections are at the desired pressure, a pneumatically driven stainless steel rod, tipped with a broad arrowhead, ruptures the diaphragm, sending a planar shock into the driven section. Four PTs, located on the top of the driven section, record the pressure pulse from the shock wave as it passes. The MCT detector and IR source are located coincident with the fourth downstream PT, providing nearly instantaneous temperature measurements immediately before and immediately after the shock. For details of experimental methods and theoretical evaluation of post-shock properties, see Materials and Methods.

Each gas mixture was tested at three driver pressures (1006, 1145, and 1282 kPa), and each of these was applied to three initial pressures (39.3, 78.6, and 118 kPa) in the driven section, providing experimental datasets at nine distinct pressure ratios (overpressures, P_r), where

[1]Mechanical Engineering Department, University of New Mexico, Albuquerque, NM 87131, USA. [2]J. Mike Walker' 66 Department of Mechanical Engineering, Texas A&M University, College Station, TX 77843, USA. [3]Department of Aeronautics and Astronautics, Air Force Institute of Technology, Wright-Patterson AFB, OH 45433, USA. [4]Aerospace Engineering Department, The Ohio State University, Columbus, OH 43210, USA. [5]Joint Institute for High Temperatures, Russian Academy of Science, Moscow 125412, Russia.
*Corresponding author. Email: patrick.j.wayne@gmail.com

pressure ratio is defined as the ratio of driver pressure to the driven pressure ($P_r = P_{driver}/P_{driven}$). Figure 1A is an experimental signal trace at a pressure ratio of P_r = 10.9, for a 50%/50% mixture of SF_6/He.

The black line shows the signal (V) from the fourth downstream PT, and the magenta line shows the signal (V) from the MCT detector. Average values of the signals from each PT are determined in a 2-ms window after shock impact (dashed blue line). This average value, combined with a calibration curve for each PT (provided by the manufacturer), provides us with the post-shock pressure, P_2 (kPa). To obtain the incident shock velocity, u_1 (m/s), the distance between two successive PTs is divided by the time it takes the shock wave to travel between them. Measurements of temperature for the MCT are obtained by taking the maximum value of the signal within the same 2-ms window (Fig. 1A). We conducted a rigorous calibration experiment with the MCT detector and IR light source to determine post-shock temperature, T_2 (K).

RESULTS

We conducted multiple experiments for each gas mixture, with a minimum of six experiments for each of the nine pressure ratios. P_r ranges from 8.54 to 32.6 for the 50/50 SF_6/He mixture and from 8.56 to 33.0 for the 25/75 SF_6/He mixture. Experimental results in Figs. 1 to 4 were produced by statistical analysis (*19*) of the dataset of measurements described above and correspond to mean values for each pressure ratio. Theoretical predictions are calculated as follows: The equations of state (EOS) are used to characterize the component gases. An ideal gas EOS is used for He, while a virial expansion—up to the fourth virial coefficient—is used for SF_6. Inputs for the EOS are the initial pressure (P_1) and temperature (T_1) in the driven section of the shock tube. Once the components have been characterized (the process includes calculations of density, specific heat ratio, thermal expansion coefficient, isothermal compressibility, and speed of sound for both He and SF_6), we use Dalton's and Amagat's laws to determine thermodynamic coefficients for the gas mixture. Specifically, we are interested in the specific

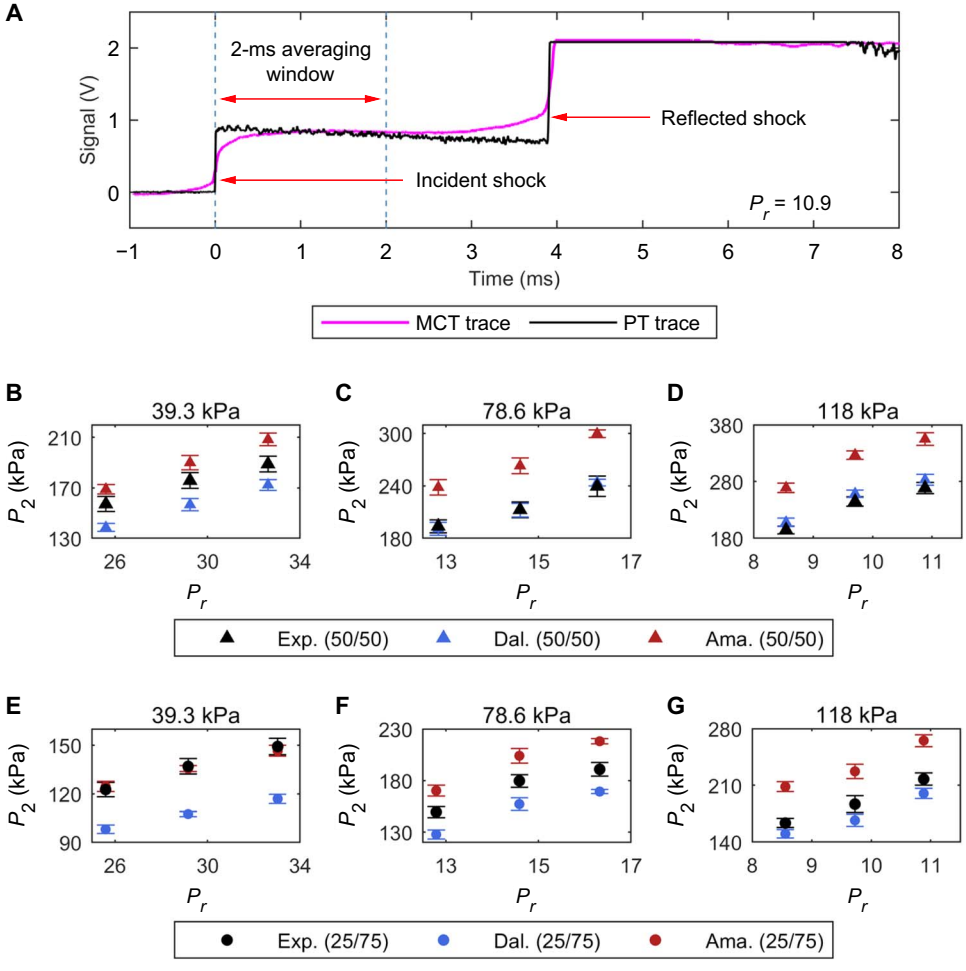

Fig. 1. Time history of recorded signals and post-shock pressure dependence on initial pressure ratio. (**A**) Sample PT and MCT detector signal traces, showing locations of incident and reflected shocks, as well as the 2-ms averaging window (dashed blue lines) used in data analysis. The black line is the signal trace from the fourth downstream PT, and the magenta line is the MCT signal trace. (**B** to **D**) Post-shock pressure, P_2, versus pressure ratio, P_r for a 50/50 (by mole) binary mixture of SF_6 and helium, respectively. (**E** to **G**) Post-shock pressure versus pressure ratio for a 25/75 binary mixture of SF_6 and helium. In all panels (B to G), black symbols correspond to experimental values, blue symbols represent Dalton's law predictions, and red symbols denote Amagat's law predictions. Vertical error bars correspond to total uncertainty in post-shock pressure P_2. Horizontal error bars are omitted as they do not extend past the physical size of the symbols. The driven pressure associated with each dataset is displayed above the corresponding panel.

heat ratio (γ) and the speed of sound (a). These values, combined with the incident shock speed (u_1), are used as inputs to the Rankine-Hugoniot equations, which are then used to determine post-shock temperature and pressure. Predictions displayed in Figs. 1 to 4 correspond to mean values for each pressure ratio. This process, and the corresponding statistical analysis, is explained in detail in Materials and Methods.

Figure 1 shows plots of post-shock pressure (P_2) versus pressure ratio (P_r) for the 50/50 mix (Fig. 1, B to D) and the 25/75 mix (Fig. 1, E to G). The corresponding initial pressures (in the driven section) are displayed above each panel (Fig. 1, B to G). Vertical error bars correspond to total uncertainty in post-shock pressure. Horizontal error bars corresponding to uncertainty in pressure ratio (P_r) do not extend past the physical size of the symbols and are therefore omitted. Note the strong disagreement not only between experimental values and theoretical predictions but also between the two mixture concentrations. Not only do these results disagree with both Dalton's law and Amagat's law well beyond experimental uncertainty, the disagreement varies with experimental value, leaving no clear answer: Which law describes the experiment better overall?

Figure 2 shows the relationship between post-shock pressure (P_2) and incident shock speed (u_1) for the 50/50 SF_6/He mixture (Fig. 2A) and the 25/75 SF_6/He mixture (Fig. 2B). In both plots, black symbols denote experimentally measured values, blue symbols correspond to Dalton's law predictions, and red symbols represent Amagat's law predictions. Vertical error bars in both plots denote total uncertainty in post-shock pressure. Horizontal error bars (on experimental values) correspond to total uncertainty in incident shock speed. Note that horizontal error bars for both Dalton's and Amagat's laws are withheld, as the uncertainty in incident shock speed for both thermodynamic laws is identical to those for experimental measurements.

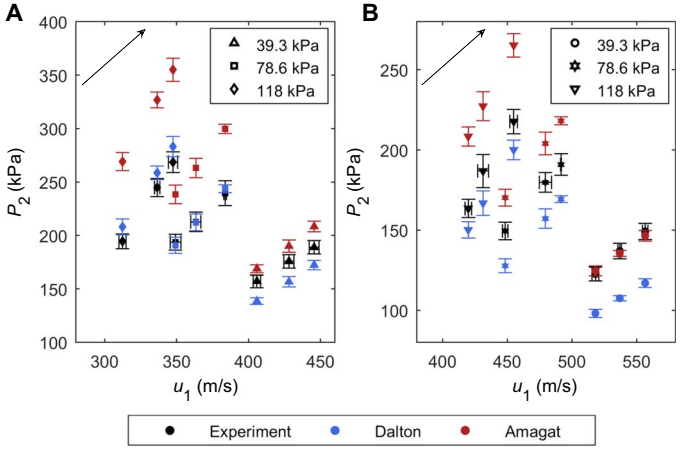

Fig. 2. Post-shock pressure variation with incident shock speed. (**A**) Post-shock pressure (P_2) versus incident shock speed (u_1) for a 50/50 (by mole) binary mixture of SF_6 to helium, respectively. (**B**) Post-shock pressure versus incident shock speed for a 25/75 binary mixture of SF_6 to helium. In both plots, experimental values are given by black symbols, blue symbols correspond to Dalton's law predictions, and red symbols represent Amagat's law predictions. Black arrows show the direction of increasing driver pressure from 1006 to 1282 kPa. Vertical error bars correspond to the total uncertainty in post-shock pressure P_2 (experimental measurements and theoretical predictions), which includes random and systematic uncertainties. Horizontal error bars correspond to total uncertainty in velocity measurements. Horizontal error bars for theoretical predictions are omitted, as the uncertainty in incident shock speed for both thermodynamic laws is identical to that of the experimental measurements.

Black arrows in Fig. 2 (A and B, upper left corner) show the direction of increasing driver pressure, from 1006 to 1282 kPa. While it seems that experimental values are closer to Dalton's law predictions for the 78.6- and 118-kPa datasets, data for 39.3 kPa are inconclusive. Again, note the discrepancies between respective initial pressures and between the two mixtures. The next step is to evaluate post-shock temperature and compare it with theoretical predictions.

Figure 3A is a plot of post-shock temperature (T_2) versus pressure ratio for the 50/50 SF_6/He mixture, and Fig. 3B is the same plot for the 25/75 SF_6/He mixture. Vertical error bars for experimental measurements and theoretical predictions correspond to total uncertainty in post-shock temperature. Note that the inputs used to calculate predictions for both Dalton's and Amagat's laws are the initial pressure (P_1) and temperature (T_1) in the driven section of the shock tube, which are measured values. Therefore, these predictions will not fit smoothly on a curve; the curve fits shown in Fig. 2 (A and B) serve merely as visual aids.

Again, there is strong disagreement between experimentally obtained values of post-shock temperature and theoretical predictions. For the 50/50 mixture, it seems that experimental values are closer to Dalton's law predictions, and for the 25/75 mixture, experimental values are closer to Amagat's law predictions; these discrepancies are not random. What could be responsible for this systematic disagreement?

DISCUSSION

A compelling theoretical analysis of finite-strength shock propagation through a binary gas mixture was published by Sherman (*20*) for inert gas mixtures consisting of argon (Ar) and He (for a range of molar concentrations of each component). Using a continuum approach, Sherman focused on determining the structure of a shock wave of arbitrary strength, which includes ordinary diffusion, barodiffusion, and thermal diffusion effects. He concluded that barodiffusion speeds up the heavier component and slows down the lighter

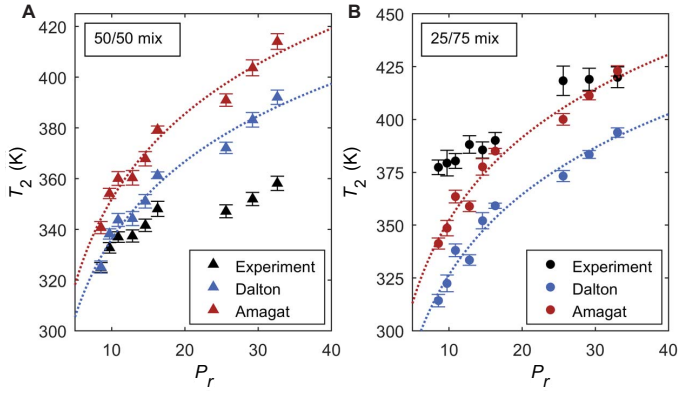

Fig. 3. Post-shock temperature dependence on initial pressure ratio. In both plots, black symbols correspond to experimental values, blue symbols represent Dalton's law predictions, and red symbols denote Amagat's law predictions. Blue and red dotted lines in both plots are curve fits to Dalton's and Amagat's law predictions, respectively; they are simply used as guides to the eye. Vertical error bars correspond to total uncertainty in post-shock temperature T_2, which includes both random and systematic uncertainties. (**A**) Post-shock temperature (T_2) versus pressure ratio (P_r) for a 50/50 binary mixture of SF_6 to helium. Here, experimental values are closer to Dalton's law predictions. (**B**) Post-shock temperature versus pressure ratio for a 25/75 binary mixture of SF_6 to helium. In contrast to data presented in (A), experimental values for a 25/75 mixture are closer to Amagat's law predictions.

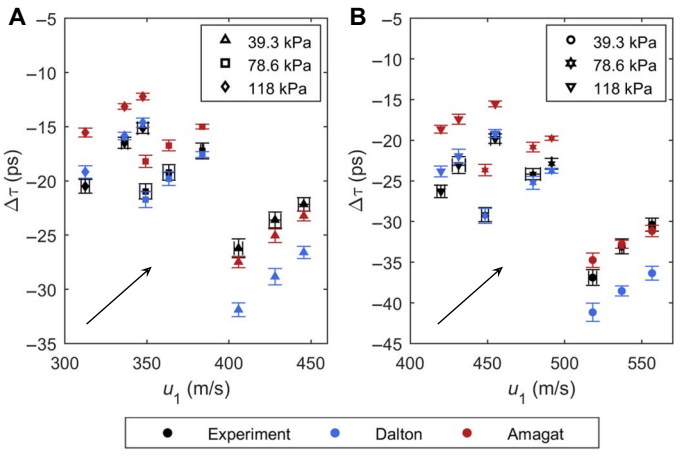

Fig. 4. Kinetic theory correlations with incident shock speed. (**A**) Change in collision time, $\Delta\tau = \tau_{He} - \tau_{SF_6}$, for a 50/50 (by mole) binary mixture of SF_6 to helium, respectively. (**B**) Change in collision time for a 25/75 binary mixture of SF_6 to helium. In both plots, experimental values are given by black symbols, blue symbols denote Dalton's law predictions, and red symbols represent Amagat's law predictions. Vertical error bars correspond to total uncertainty in $\Delta\tau$, and horizontal error bars correspond to total uncertainty in velocity measurements. Similar to Fig. 2, horizontal error bars for theoretical predictions are omitted, and black arrows show the direction of increasing driver pressure from 1006 to 1282 kPa. These data closely resemble the trends we observe above (Figs. 1 to 3).

Table 1. Statistical information of experimental measurements for a 50/50 binary mixture of SF_6 and helium, where n is the number of samples, ν is the degrees of freedom (combined or otherwise), and t is the Student's t distribution value.

P_r (50/50)	n_{P_2}	ν_{P_2}	t_{P_2}	n_{u_1}	ν_{u_1}	t_{u_1}	n_{T_2}	ν_{T_2}	t_{T_2}
32.61	15	6	2.4469	5	4	2.7764	5	4	2.7764
16.27	23	10	2.2281	4	3	3.1824	7	6	2.4469
10.88	20	10	2.2281	6	5	2.5706	5	4	2.7764
29.24	20	16	2.1199	5	4	2.7764	6	5	2.5706
14.60	21	11	2.2010	5	4	2.7764	5	4	2.7764
9.70	21	10	2.2281	5	4	2.7764	6	5	2.5706
25.60	22	15	2.1314	6	5	2.5706	6	5	2.5706
12.83	22	15	2.1314	5	4	2.7764	6	5	2.5706
8.54	22	17	2.1098	6	5	2.5706	6	5	2.5706

component relative to the mass velocity of the mixture (*20*). He also determined that thermal diffusion will have the opposite effect, slowing down the heavier component and speeding up the lighter one. Therefore, thermal diffusion would (at least partially) counteract barodiffusion within the shock wave. Sherman calculated his results through numerical integration of the Navier-Stokes equations. A primary assumption associated with this analysis was always imposing thermal equilibrium between species through the shock wave. However, Sherman indicates that these assumptions (and corresponding analysis) may not be valid for strong shock waves, or for mixtures with large molecular mass ratios. He states that one might intuitively expect that the maximum shock strength for which these calculations give realistic predictions would be reduced (somewhat significantly) as the molecular mass ratio increases because of the difficulty in maintaining thermal equilibrium between the gas components (*20*).

In 1967, Bird (*21*) produced an interesting attempt to model shock propagation through a binary mixture of 50/50 Ar-He, representing the gas molecules as rigid elastic spheres—with the appropriate masses and diameters—and compared his results with the analytical predictions of Sherman. His model did not have the same temperature constraints as Sherman and predicted even greater differences in velocity, temperature, and concentration profiles than the analytical profiles of Sherman. Furthermore, Bird's findings suggest that the temperature non-equilibrium between species increases with low concentrations of the heavy gas component and that this (non-equilibrium) can persist for a considerable distance downstream of the shock (*21*). For reference, the molecular mass ratio with respect to binary mixtures of Ar-He is approximately 10, while the molecular mass ratio associated with the current work (SF_6-He) is around 36.5.

The studies conducted by Sherman and Bird reasonably concluded that shock propagation through gas mixtures with relatively massive molecules would cause differences in their behavior, but the results only pertained to gas molecule velocity, concentration, and temperature profiles—on time (and length) scales much smaller than these considered in the current work. Perhaps the results shown in Figs. 1 to 3, taken in context with these early studies, suggest a different explanation, beyond experimental uncertainty.

Is a kinetic molecular theory (KMT) (*22*, *23*) explanation possible? Dalton's and Amagat's laws predate KMT, but each law makes implicit assumptions about reversibility. Both laws assume thermodynamic equilibrium. However, while Dalton's law assumes that the gases are always perfectly mixed, Amagat's law assumes that the gases will separate over time. This assertion is interesting because that is exactly what we see in experiments. The molecular mass of SF_6 is approximately 36.5 times greater than that of He. If the gases are not constantly mixed, then they will begin to separate (under normal conditions, the gases will separate within a few minutes). Before taking measurements described here, our initial guess was that Amagat's law might provide a better prediction for these dissimilar gases. The time scale of that separation, however, is much longer than that of the experiment associated with the shock passage, thus leading to both Dalton's law (infinite separation time) and Amagat's law (the gases in the mixture are in effect always separated) failing to produce a match with experiment.

What relaxation time scale is relevant for the equilibrium status of a shocked gas mixture? Relaxation time is defined as the time within which a perturbed gas will reach statistical (thermodynamic) equilibrium (*24*). In binary gas mixtures whose constituents have widely different molecular masses ($M_{SF_6} \gg M_{He}$), disparate relaxation times are manifest, governing the approach to equilibrium of the various degrees of freedom (*25*). According to Mora and Fernández-Feria (*25*), for such mixtures, the process of equilibration can be characterized by three different relaxation times: two for self-equilibration of the component gases and a third one associated with the slower process of interspecies equilibration. For this analysis, these relaxation times are the post-shock mean free time (or average time between molecular collisions) for each of the gas components (τ_{He} and τ_{SF_6}) and the change in collision time between them ($\Delta\tau = \tau_{He} - \tau_{SF_6}$). What is

Table 2. Statistical information of experimental measurements for a 25/75 binary mixture of SF_6 and helium, where *n* is the number of samples, ν is the degrees of freedom (combined or otherwise), and *t* is the Student's *t* distribution value.

P_r (25/75)	n_{P_2}	ν_{P_2}	t_{P_2}	n_{u_1}	ν_{u_1}	t_{u_1}	n_{T_2}	ν_{T_2}	t_{T_2}
33.03	20	12	2.1788	6	5	2.5706	6	5	2.5706
16.32	24	20	2.0860	4	3	3.1824	5	4	2.7764
10.88	18	8	2.3060	6	5	2.5706	6	5	2.5706
29.16	28	21	2.0796	6	5	2.5706	6	5	2.5706
14.59	19	10	2.2281	6	5	2.5706	6	5	2.5706
9.73	21	12	2.1788	6	5	2.5706	6	5	2.5706
25.59	21	11	2.2010	6	5	2.5706	6	5	2.5706
12.79	20	13	2.1604	4	3	3.1824	6	5	2.5706
8.56	18	10	2.2281	6	5	2.5706	6	5	2.5706

remarkable about this method is that the mean free time is temperature and pressure dependent (see Materials and Methods).

Figure 4 is a plot of the change in collision time, Δτ (in picoseconds), versus incident shock velocity (u_1) for the 50/50 SF_6/He mixture (Fig. 4A) and the 25/75 SF_6/He mixture (Fig. 4B). Symbol type and color in Fig. 4 have been arranged similar to Fig. 2. Again, the black arrow in both plots points in the direction of increasing driver pressures. Note again the systematic discrepancies in these data, consistent with the spread of experimental data points. The negative values for Δτ are due to the fact that the average collision time for SF_6 is an order of magnitude greater than that of He. While Figs. 1 to 3 show discrepancies produced by Dalton's and Amagat's laws in predicting post-shock properties (pressure and temperature) on a macroscopic scale, Fig. 4 provides a context for these discrepancies, relating them to the simplest quantitative parameter describing the disparity between component gas behavior on a microscopic scale. Therefore, if the component gases behave differently, i.e., have a large difference in response time, on a microscale, is it not reasonable to assume that these discrepancies manifest on a macroscale? This hypothesis is reinforced by the results obtained from Sherman (*20*) and Bird (*21*), especially considering the large molecular mass difference between the species.

The simple explanation that KMT can provide is that differences in the response time of the molecules account for the disagreement between theory and experiment. This explanation appears to agree with our data, at least qualitatively. These observations show that Dalton's and Amagat's laws fail to accurately describe the behavior of a gas mixture that underwent shock acceleration, with implications that the same failure can manifest in other non-equilibrium situations.

MATERIALS AND METHODS

Experimental setup

Two gas mixtures were tested: 50%/50% and 25%/75% SF_6 to He, by mole, respectively. Experiments were conducted at the Shock Tube Facility in the Mechanical Engineering Department at the University of New Mexico. The shock tube itself is approximately 5.2 m long with a 2-m-long driver section and a 3.2-m-long driven section (7.62 cm inside square cross-section).

To begin an experiment, we separated the driver and driven sections of the shock tube with a thin-film polyester diaphragm. Both sections were then evacuated using an ITT Pneumotive vacuum pump to −78.6 kPa. The driven (test) section was filled with the test mixture to a predetermined pressure (39.3, 78.6, or 118 kPa). The driver was filled with nitrogen to another predetermined pressure (1006, 1145, or 1282 kPa). The pressure in the driver section depends on the desired strength (or Mach number) of the shock wave (*2*). Once the pressure in both sections has stabilized, a pneumatically driven stainless steel rod tipped with a broad arrowhead punctures the diaphragm, sending a normal shock down the length of the driven section. Four PTs (with a response time of ≤1 μs), located on the top of the driven section (≈ 0.8 m apart), record the pressure history of the shock wave as it passes. These data can then be used to determine the velocity of the shock wave, u_1, and the post-shock pressure, P_2. The MCT detector and IR source were placed on opposite sides of the shock tube, perpendicular to the optical axis and located coincident with the fourth downstream PT. Two zinc selenide (ZnSe) optical windows were placed on either side of the shock tube, mounted flush with the inside of the test section. These optical windows were used to create an airtight, unobstructed light path from the IR source, through the test gas in the driven section, to the sensor on the MCT detector. They were also used as broadband filters to decrease the wavelength range of the incoming light from the IR source to between 7 and 12 μm (the IR source outputs light between 0.5 μm and approximately 20 μm). A germanium notch filter, mounted on the MCT detector itself, further reduces the range of incoming light to between 7.5 and 9.0 μm. Note that the target range for these experiments was chosen to be between 7.5 and 8.5 μm, on the basis of the IR absorption spectrum of SF_6 (*26*).

Calibration curves that relate the signal (V) from the PTs to pressure (kPa) in the driven section were provided for each transducer by the manufacturer. For the MCT detector, a calibration experiment was conducted to determine the relationship between signal (V) and temperature (K). This experiment used an aluminum cylinder with ZnSe optical windows mounted on each side, with components and geometry identical to that of the shock tube setup described above. The cylinder chamber was evacuated with a vacuum pump and filled with the test gas mixture at a prescribed pressure [target pressures were determined from previous experiments (*27*)]. A helical coil resistance heater, placed on the inside of the calibration cylinder, was then activated to increase the temperature of the test gas to a predetermined value. A Vincent Associates Uniblitz LS6 laser shutter (6-mm aperture, 1.7-ms open time) was placed along the optical axis in front of the MCT detector, which effectively simulates an instantaneous increase in temperature, as would be seen by the sensor when the shock wave passes (*2*). Once the laser shutter was activated, the signal from the detector was recorded and used as a baseline for that pressure-temperature (P-T) combination. For each gas mixture, data were obtained at up to 25 P-T combinations, with a minimum of six measurements at each combination. This method provided ample data to determine a calibration curve for each gas mixture.

Thermodynamic models

The following theoretical analysis was used to determine post-shock pressure and temperature for both Dalton's and Amagat's laws. EOS

are needed to characterize the gas components; the Ideal Gas (Eq. 1) EOS was used for He, and a virial expansion (Eq. 2) was used for SF_6

$$Pv = RT \tag{1}$$

$$P = \frac{RT}{v}\left(1 + \frac{B(T)}{v} + \frac{C(T)}{v^2} + \frac{D(T)}{v^3} + \frac{E(T)}{v^4}\right) \tag{2}$$

Here, P is the pressure (N/m^2), v is the specific volume (m^3/mol), R = 8.314 J/mol·K is the universal gas constant, T is the temperature (K), $B(T)$ is the second virial coefficient, $C(T)$ is the third virial coefficient, and so forth (*28*). Algebraic expressions of the temperature provided by the hard-core square well model intermolecular potential are used to represent $B(T)$ and $C(T)$, while $D(T)$ and $E(T)$ are represented as polynomial functions of the inverse temperature (*29*)

$$B(T) = b_0[1 - (\lambda^3 - 1)\Delta] \tag{3}$$

$$C(T) = \frac{1}{8}b_0^2(5 - c_1\Delta - c_2\Delta^2 - c_3\Delta^3) \tag{4}$$

$$D(T) = \sum_{n=0}^{3} d_n T^{-n} \tag{5}$$

$$E(T) = \sum_{n=0}^{3} e_n T^{-n} \tag{6}$$

where $\Delta = e^{\epsilon/k_b}T - 1$ (k_b is Boltzmann's constant) and the coefficients c_1, c_2, and c_3 are given by

$$c_1 = \lambda^6 - 18\lambda^4 + 32\lambda^3 - 15 \tag{7}$$

$$c_2 = 2\lambda^6 - 36\lambda^4 + 32\lambda^3 + 18\lambda^2 - 16 \tag{8}$$

$$c_3 = 6\lambda^6 - 18\lambda^4 + 18\lambda^2 - 6 \tag{9}$$

Values for d_n (n = 1,2,3), e_n (n = 1,2,3), b_0, λ, and ϵ/k_b are provided by Hurly *et al.* (*29*).

Inputs for the EOS are the initial pressure (P_1) and temperature (T_1) of the test gas in the driven section. Once the component gases have been characterized, we used Dalton's law and Amagat's law to determine thermodynamic coefficients for the mixture. We were specifically looking for the speed of sound, a, and the specific heat ratio, γ. These variables, coupled with the incident shock speed u_1 (determined from experiment) were used as inputs for the Rankine-Hugoniot equations (Eqs. 10 to 13), which relate post-shock properties in terms of initial conditions (preshock) and incident shock Mach number M_1

$$M_1 = \frac{u_1}{a} \tag{10}$$

$$M_2^2 = \frac{M_1^2 + 2/(\gamma - 1)}{[2\gamma/(\gamma - 1)]M_1^2 - 1} \tag{11}$$

$$T_1\left(1 + \frac{\gamma - 1}{2}M_1^2\right) = T_2\left(1 + \frac{\gamma - 1}{2}M_2^2\right) \tag{12}$$

$$\frac{P_1}{P_2} = \frac{1 + \gamma M_2^2}{1 + \gamma M_1^2} \tag{13}$$

The subscripts 1 and 2 correspond to conditions before and after the shock, respectively. Once the post-shock temperature (T_2) and pressure (P_2) for each thermodynamic law (Dalton and Amagat) have been calculated, we can directly compare the results with experimental values. All theoretical calculations and analysis of experimental data (including statistical analysis) were performed in MATLAB.

Kinetic molecular theory

Central to KMT are the following assumptions (*30*):

(1) The size of the particle is negligibly small; i.e., the particles themselves occupy no volume, even though they have mass. At the maximum concentration of molecules in our experiments, the Van der Waals correction to pressure associated with molecular volume would not exceed 2.5%.

(2) The average kinetic energy of a particle is proportional to the temperature (K).

(3) Particle collisions are perfectly elastic; they may exchange energy, but there is no overall loss of energy.

The following equations were used for kinetic theory analysis. The mean free path (l) is given by

$$l = \frac{k_b T}{\sqrt{2}\pi d^2 P} \tag{14}$$

where $k_b \approx 1.381 \times 10^{-23}$ m^2 kg s^{-2} K^{-1} is the Boltzmann constant, T is the temperature (K), d is the kinetic diameter, which is 0.260 $\times 10^{-9}$ m for He and 0.550 $\times 10^{-9}$ m for SF_6, and P is the pressure (Pa).

Mean molecular speed (μ_m) is obtained via

$$\mu_m = \sqrt{\frac{8TR_s}{\pi}} \tag{15}$$

where R_s is specific gas constant: for He, $R_s = 2.0773 \times 10^{-3}$ J/kg·K, and for SF_6, R_s = 56.9269 J/kg·K.

Average collision time (τ) is calculated using

$$\tau = \frac{l}{\mu_m} \tag{16}$$

The change in average collision time, Δτ, is simply the average collision time of He, τ_{He}, minus the average collision time of SF_6, τ_{SF_6}

$$\Delta\tau = \tau_{He} - \tau_{SF_6} \tag{17}$$

Statistical analysis

A comprehensive statistical analysis was performed on all experimental data, according to steps outlined by Wheeler and Ganji (*19*). Statistical analysis on all measurements (pressure, temperature, and velocity) begins with outlier rejection using the Modified Thompson

Tau technique (*19*). In this method, for any n measurements, with a mean value $\bar{x}$ and SD S, the data are arranged in ascending order ($x_1, x_2, ...,x_n$). The extreme (highest and lowest) values are suspected outliers. For these suspected points, a deviation is calculated as

$$\delta_i = |x_i - \bar{x}| \tag{18}$$

and the largest value is selected. This value is compared with the product of τ (tabulated with respect to n) times the SD S. If the value of δ exceeds τS, then this value can be rejected as an outlier (only one value is eliminated for each iteration). The mean and SD of the remaining values are then recomputed, and the process is repeated until no more outliers exist. Note that n decreases with each outlier rejection.

Pressure measurements were obtained using multiple devices. Therefore, an estimation of the combined degrees of freedom according to the Welch-Satterthwaite formula (Eq. 18) is necessary (*19*).

$$\nu_x = \frac{\left[\sum_{i=1}^{m} S_i^2\right]^2}{\sum_{i=1}^{m} (S_i^4/\nu_i)} \tag{19}$$

where ν_i is the degrees of freedom for the measuring device and ν_x is the value of the combined degrees of freedom for variable x. Degrees of freedom for temperature and velocity measurements are simply $\nu_x = n - 1$. When ν_x has been determined, Student's t distribution value (t) is found on the basis of a 95% level of confidence. The total random uncertainty in the mean value $P_{\bar{x}}$ is computed by

$$P_{\bar{x}} = \pm \frac{S_x}{\sqrt{n}} \tag{20}$$

where $S_x/\sqrt{n}$ is the estimate of the SD of the mean.

Systematic uncertainty for each variable is determined using the mean value for the measurement and manufacturer-supplied information, such as linearity, hysteresis, and uncertainty in the measuring device. Sources of systematic error are PTs, pressure gauges, oscilloscopes, and the MCT detector. Total systematic error is given by

$$B_x = \left[\sum_{i=1}^{k} B_i^2\right]^{1/2} \tag{21}$$

where B_i is the systematic error for measuring device i. Once all sources of random and systematic error have been determined, the total uncertainty in the mean ($W_{\bar{x}}$) is given by

$$W_{\bar{x}} = (B_x^2 + P_{\bar{x}}^2)^{1/2} \tag{22}$$

The mean value for a given set of measurements is used in all plots, and error bars represent total uncertainty (±) in the mean value.

Table 1 details the number of measurements n, degrees of freedom ν (combined or otherwise), and the t distribution value for post-shock pressure (P_2), incident shock speed (u_1), and post-shock temperature (T_2) for the 50/50 binary mixture of SF_6 and He. P_r denotes the pressure ratio according to mean values of driver and driven pressures for a given set of experiments. Table 2 details statistics for a 25/75 mixture of SF_6 and He. All statistical analysis was performed in MATLAB.

REFERENCES AND NOTES

1. J. Dalton, Essay IV. On the expansion of elastic fluids by heat. *Mem. Proc. Manch. Lit. Philos. Soc.* **5**, 595–602 (1802).
2. P. Wayne, S. Cooper, D. Simons, I. Trueba-Monje, J. H. Yoo, P. Vorobieff, C. R. Truman, S. Kumar, Investigation of Dalton's and Amagat's laws for gas mixtures with shock propagation. *Int. J. Comput. Methods Exp. Meas.* **6**, 1–10 (2017).
3. Y. Çengel, J. Cimbala, R. Turner, *Fundamentals of Thermal-Fluid Sciences* (McGraw-Hill, 2011).
4. L. Bernstein, Tabulated solutions of the equilibrium gas properties behind the incident and reflected normal shock-wave in a shock tube (C.P. No. 626, Ministry of Aviation, Aeronautical Research Council Current Papers, 1963).
5. L. Davies, D. Edwards, An experimental investigation of the reflected-shock pressure-time profiles in air, oxygen, nitrogen, argon, carbon dioxide and acetylene (R. & M. No. 3446, Ministry of Aviation, Aeronautical Research Council Reports and Memoranda, 1967).
6. M. S. El-Genk, J.-M. Tournier, Noble gas binary mixtures for gas-cooled reactor power plants. *Nucl. Eng. Des.* **238**, 1353–1372 (2008).
7. J. Diaz, Preface gaseous core reactors. *Nucl. Technol.* **69**, 129–133 (2017).
8. A. Ferri, G. Moretti, S. Slutsky, Mixing processes in supersonic combustion. *J. Soc. Ind. Appl. Math.* **13**, 229–258 (1965).
9. C. Gruenig, F. Mayinger, Supersonic combustion of kerosene/H_2-mixtures in a model scramjet combustor. *Combust. Sci. Technol.* **146**, 1–22 (1999).
10. J.-x. Tao, Studies of a combined way of flame stability in ramjet combustor. *Def. Technol.* **14**, 441–445 (2018).
11. F. Marble, E. Zukoski, J. Jacobs, G. Hendricks, I. Waitz, Shock enhancement and control of hypersonic mixing and combustion. *American Institute of Aeronautics and Astronautics*, AIAA 90–1981 (1990).
12. P. Lorén-Aquilar, M. Bate, Two-fluid dust and gas mixtures in smoothed particle hydrodynamics II: An improved semi-implicit approach. *Mon. Not. R. Astron. Soc.* **454**, 4114–4119 (2015).
13. R. Anand, On dynamics of imploding shock waves in a mixture of gas and dust particles. *Int. J. Nonlin. Mech.* **65**, 88–97 (2014).
14. F. White, *Fluid Mechanics* (McGraw-Hill, 2003).
15. R. Zucker, O. Biblarz, *Fundamentals of Gas Dynamics* (Wiley, 2002).
16. E. Goldman, L. Sirovich, The structure of shock-waves in gas mixtures. *J. Fluid Mech.* **35**, 575–597 (1969).
17. J. Anderson, *Modern Compressible Flow with Historical Perspective* (McGraw-Hill, 1982).
18. J. John, *Gas Dynamics* (Prentice Hall, 1984).
19. A. Wheeler, A. Ganji, *Introduction to Engineering Experimentation* (Prentice Hall, 2010).
20. F. Sherman, Shock-wave structure in binary mixtures of chemically inert perfect gases. *J. Fluid Mech.* **8**, 465–480 (1960).
21. G. A. Bird, The structure of normal shock waves in a binary gas mixture. *J. Fluid Mech.* **31**, 657–668 (1968).
22. L. Loeb, *The Kinetic Theory of Gases* (Dover Publications, 1961).
23. C. Collie, *Kinetic Theory and Entropy* (Longman Inc., 1982).
24. L. Landau, E. Lifshitz, *Statistical Physics* (Pergamon Press, 1980).
25. J. Mora, R. Fernández-Feria, Kinetic theory of binary gas mixtures with large mass disparity. *Phys. Fluids* **30**, 740 (1987).
26. R. Lagemann, E. Jones, The infrared spectrum of sulfur hexafluoride. *J. Chem. Phys.* **19**, 534–536 (1951).
27. I. Trueba-Monje, J. Yoo, paper presented at the AIAA Region IV Student Conference, Houston, TX, April 2016.
28. H. Callen, *Thermodynamics and An Introduction to Thermostatistics* (Wiley, 1985).
29. J. Hurly, D. Defibaugh, M. Moldover, Thermodynamic properties of sulfur hexafluoride. *Int. J. Thermophys.* **21**, 739–765 (2000).
30. N. Tro, *Chemistry: A Molecular Approach* (Prentice Hall, 2011).

Acknowledgments: We thank J. Bigelow for comments, suggestions, and numerical work. **Funding:** P.W., S.C., D.S., I.T.-M., D.F., and G.V. acknowledge support from the National Nuclear Security Administration (NNSA) grant DE-NA-0002913. **Author contributions:** P.W. conducted the shock tube and calibration experiments, analyzed the data, performed uncertainty analysis, and wrote the paper. S.C. and D.S. helped with data collection and analysis on both the calibration and shock tube experiments. I.T.-M. helped with preliminary shock tube experiments and data collection. D.F. and G.V. helped with the calibration experiment data collection. T.C. contributed to mixing models. V.V. contributed to kinetic theory. P.V. and C.R.T. managed and supervised the process. All of the authors helped with editing the paper. **Competing interests:** The authors declare that they have no competing interests. **Data and materials availability:** All data needed to evaluate the conclusions in the paper are present in the paper. Additional data and corresponding MATLAB scripts used to support the findings in this study are available upon request from the corresponding author.

Submitted 26 March 2019
Accepted 19 September 2019
Published 6 December 2019
10.1126/sciadv.aax4749

Citation: P. Wayne, S. Cooper, D. Simons, I. Trueba-Monje, D. Freelong, G. Vigil, P. Vorobieff, C. R. Truman, V. Vorob'ev, T. Clark, Dalton's and Amagat's laws fail in gas mixtures with shock propagation. *Sci. Adv.* **5**, eaax4749 (2019).